Proceedings of the ASME 2018 International Design Engineering Technical Conferences and Computers and Information in Engineering Conference IDETC/CIE 2018
August 26-29, 2018, Quebec City, Quebec, Canada

DETC2018-85504

MOLECULAR DYNAMICS SIMULATIONS ON THE TENSILE DEFORMATION AND FAILURE OF A POLYETHYLENE/COPPER INTERFACE

Lijuan LIAO [1]*
[1] Key Laboratory for Mechanics in Fluid Solid Coupling Systems, Institute of Mechanics, Chinese Academy of Sciences, Beijing, 100190, China
E-mail: ljl@imech.ac.cn

Changyu MENG [1,2]
[1] Key Laboratory for Mechanics in Fluid Solid Coupling Systems, Institute of Mechanics, Chinese Academy of Sciences, Beijing, 100190, China
[2] School of Engineering Science, University of Chinese Academy of Sciences, Beijing, 100049, China
E-mail: mengchangyu@imech.ac.cn

Chenguang HUANG [1,2]
[1] Key Laboratory for Mechanics in Fluid Solid Coupling Systems, Institute of Mechanics, Chinese Academy of Sciences, Beijing, 100190, China
[2] School of Engineering Science, University of Chinese Academy of Sciences, Beijing, 100049, China
E-mail: huangcg@imech.ac.cn

ABSTRACT

In this study, a microscale interface consisting of amorphous polyethylene (PE) chains with the united-atom (UA) model and face-centered cubic (FCC) crystal copper as the substrate was established. Moving the copper layer with a given rate, the damage evolution of the interface during the tensile deformation was examined by molecular dynamics (MD) simulations. The stress-strain relationship was obtained to capture the evolution of tensile deformation. The distribution of the temperature field was adopted to predict the damage initiation and the failure mode. The phase diagram of the failure mode with respect to the thickness of the PE layer and the loading rate was provided. The results show that the PE layer with smaller thickness brings higher load-bearing capacity with larger yield strength. As for the rate-dependence, a rate-hardening followed by a rate-softening of yield strength was observed. In addition, the failure modes evolves from cohesive failure to interfacial one as the loading rate of tension increases progressively. It can be assumed that the control parameter on the failure mode changes from pure material strength of PE to the bonding strength between PE and copper. Furthermore, a larger thickness of PE layer leads to the cohesive failure with higher probability under a narrow range of loading rate with small values. However, the thickness-dependence of failure mode attenuates gradually and diminishes ultimately under higher loading rate, which leads to the transformation from mixed mode to interfacial one.

INTRODUCTION

Connecting the similar/dissimilar materials, the interfaces formed by the physical and chemical reactions between two phases are common in industries [1], like bonding structures with adhesives, coatings etc. The mechanical performances of the interface are vital to determine the behaviors of the structures. As for the adhesive joint including polymer and metal, the crack generally initiates in the adhesive layer or in the vicinity near the interface. In addition, owing to the complex characterization of polymer, the mixed failure is the most common [2].

Many investigations [3-6] had studied the failure of the adhesive structures numerically and experimentally at macroscale. However, rather than the aggregation and propagation of the micro-voids, fibrillation occurs [7] without clear mechanism. It is still difficult to clarify the mechanism of amorphous complex structures using continuum mechanical evaluation only.

Alternatively, molecular dynamics (MD) simulation is an ideal method to examine the essential effects of microstructures on mechanical behaviors of the system consisting polymers to provide atomistic descriptions [8-10]. It provides a possibility to bridge and develop to higher length scale as meso- and continuum models [11] with intrinsic understandings.

In addition, the thickness-dependence on the interfacial strength was discussed previously [12-14]. However, except as the geometrical effect, the constraint effect [15] of walls results in the microstructure evolution is also necessary to discussed further. Especially with extreme small thickness as a thin film, the examinations in microscale viewpoint are necessary.

For simplicity, linear polyethylene (PE) chains without branching were chosen as the polymer material without taking the crosslink into account. In addition, as the common metal material in microelectronic device packaging, copper [16] was selected as the substrate. Correspondingly, a microscale interface between the two materials was built. The tensile deformation from the initiation of the micro-damage to the complete failure was simulated by MD. The evolution of stress-strain relationship was described. In addition, the temperature field of PE layer was adopted to predict the damage initiation and failure mode, which was calculated according to the velocity distribution. A parameter to classify the failure mode was also introduced. Finally, the effects of thickness of PE layer and the loading rate on the yield strength and the failure mode were discussed.

SIMULATION METHOD

A schematic flowchart of modeling, relaxation and tensile process of PE/Copper interface is plotted in Fig. 1. A single PE chain was built as a chain with one-hundred-fifty 'united atoms' (UA), each of which is a -[-CH_2-]- monomer. All visualizations in this paper were implemented by *OVITO* [17]. The time step in the simulations is 1fs.

PE chains were placed randomly into a box with an initial size of $H \times L \times W$ by *Packmol* coding [18] in R-I. The total energy of the system was calculated by Eq. (1). Each component was expressed in Eqs. (2)~(5) to describe the intra- and inter-molecular interactions of the PE chains.

During R-II, the PE box in the *z*-direction was fixed with the non-bond interactions. The corresponding potential parameters are the same to those in describing the interactions between PE UA and copper atoms. Each copper layer was defined as a rigid part ignoring the internal interactions between inner atoms. The interatomic interactions between PE UA and copper atoms were also described by the Lennard-Jones (LJ)

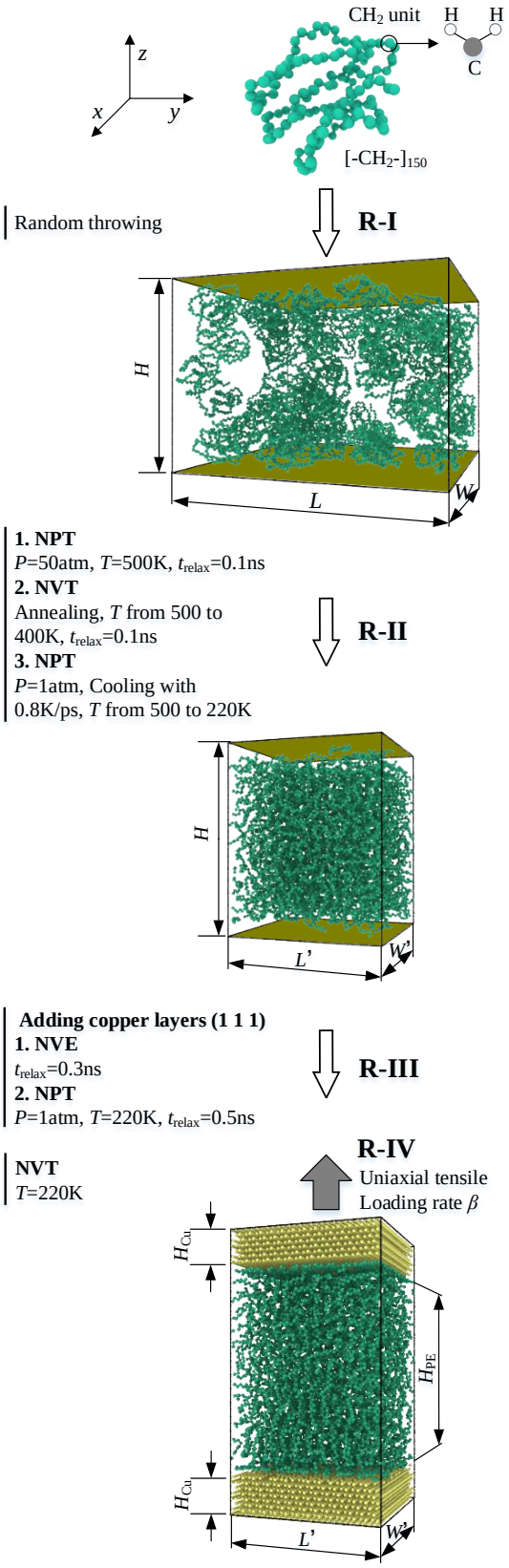

Figure 1. Schematic flowchart of modeling, relaxation and tensile process of PE/Copper interface.

12-6 potential (Eq. (5)) with a cut-off radius 10Å using the arithmetic mixing rule (Eq. (6)).

Total energy:

$$E_{\text{total}}=E_{\text{bond}}(r)+E_{\text{angle}}(\theta)+E_{\text{dihedral}}(\phi)+E_{\text{non-bond}}(r) \quad (1)$$

Bond stretching:

$$E_{\text{bond}}=\frac{1}{2}K_{\text{b}}(r-r_0)^2 \quad (2)$$

Angle bending:

$$E_{\text{angle}}=\frac{1}{2}K_{\theta}(\theta-\theta_0)^2 \quad (3)$$

Dihedral rotation:

$$E_{\text{dihedral}}(\phi)=\sum_{i=0}^{3}C_i(\cos\phi)^i \quad (4)$$

Non-bond energy:

$$E_{\text{non-bond}}(r)=4\varepsilon\left[\left(\frac{\sigma}{r}\right)^{12}-\left(\frac{\sigma}{r}\right)^{6}\right],\ r\le r_{\text{c}} \quad (5)$$

Mixing rule:

$$\varepsilon_{\text{cp}}=\sqrt{\varepsilon_{\text{Cu}}\varepsilon_{\text{PE}}},\ \sigma_{\text{cp}}=\frac{\sigma_{\text{Cu}}+\sigma_{\text{PE}}}{2} \quad (6)$$

where, K_{b} and K_{θ} are the stiffness coefficients of bond stretching and angle bending potentials, respectively. In addition, r_0 and θ_0 are the equilibrium bond length and angle, respectively. C_i (i=1, 2 and 3) is the coefficient in Eq. (4) to describe the dihedral angle. σ in Eq. (5) is the equilibrium distance between atoms as the potential energy is minimum for $r=2^{1/6}\sigma$. The necessary potential parameters in the simulations implemented in LAMMPS [19] were referred to the works of Hossain et al. [10], Shepherd [20], Huang et al. [21] and Heinz et al. [22].

Fixing the lower copper layer, the uniaxial tensile loading was provided by moving the upper one with a rate β (eleven values from 1.0 to 5.0Å/ps with an interval of 0.4Å/ps were chosen in this study) in R-IV. The equivalent strain rate ranges approximately from 10^{10}/s to 12.5×10^{10}/s.

Eight systems, which are denoted as Si (i=1, 2, …, 8), with different thicknesses of PE layer H_{PE} ranging from 40 to 110Å with an interval of 10Å were prepared. In addition, six samples were established with a unique configuration for each system to carry out a statistical analysis.

As the constitutive relation of a material [11], the interatomic potentials govern the local and global mechanical behaviors. It is worthwhile to note that both model-form uncertainty and parameter uncertainty in MD simulations exist as the results of different approximations & assumptions in the models and first principles calculations & approximated from experimental data [23]. Paul et al. [24] presented an optimized UA model of PE. Each potential component experienced adjustment to meet individual requirement. Furthermore, this study focus on the failure mechanism of bi-material interface. Accordingly, a harmonic bond potential in Eq. (2) [10, 21, 25-29], a harmonic angle potential in Eq. (3) [10, 21, 26-28], a multi-harmonic dihedral potential in Eq. (4) [10, 21, 25] and a LJ 12-6 potential in Eq. (5) [10, 21, 25, 27, 28] was adopted. These potentials were applied successfully in reproducing the mechanical responses [10, 21, 25, 26], crystallization under deformation [27], thermal transport [28] and detachment dynamics [29] of PE with reasonable and reliable results. In addition, the locations and velocities of particles at equilibrium of a system (H_{PE}≈80Å, β=1.0Å/ps) as an example were also examined taking the input uncertainty into account, which were illustrated in strain-stress curves as shown in Fig. 2. Each solid line and the corresponding shading are the average value and error band, respectively. It can be assumed that the potentials and corresponding parameters selected are acceptable.

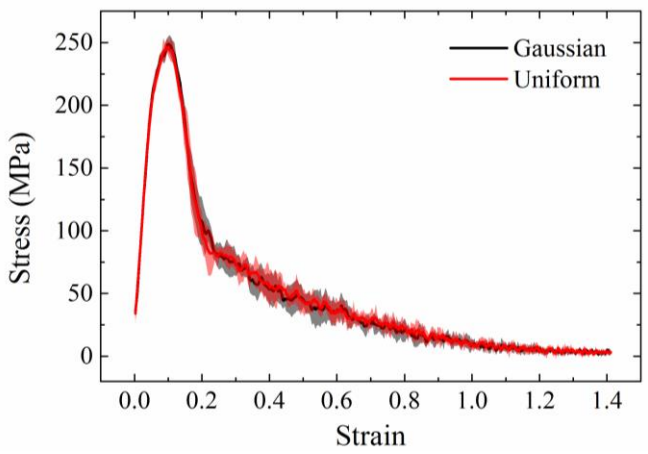

Figure 2. Sensitivity analysis of random velocity distribution of initial particles on strain-stress curve.

RESULTS AND DISCUSSIONS

The evolutions of stress-strain relationship in S3 (H_{PE}≈60Å) under β=1.8Å/ps and β=3.0Å/ps were plotted in Fig. 3 (a) as an example. The solid lines and the corresponding shading areas are the average values and the error-bands by the statistical analysis, respectively. At the global yield point, the values of stress were denoted as yield strength σ_y. An elastic region was observed with a linear rise of the stress as the strain increases. Cross the yield point, the stress declines gradually toward to zero from damage initiation to the complete failure.

As the two examples shown in Fig. 3 (b), the yield strength σ_y decreases as the thickness of PE layer H_{PE} increases. The inversely proportional relation can be obtained under given loading rate discussed in the current simulation from 1.0 to 5.0Å/ps, which consists with the results in the previous MD

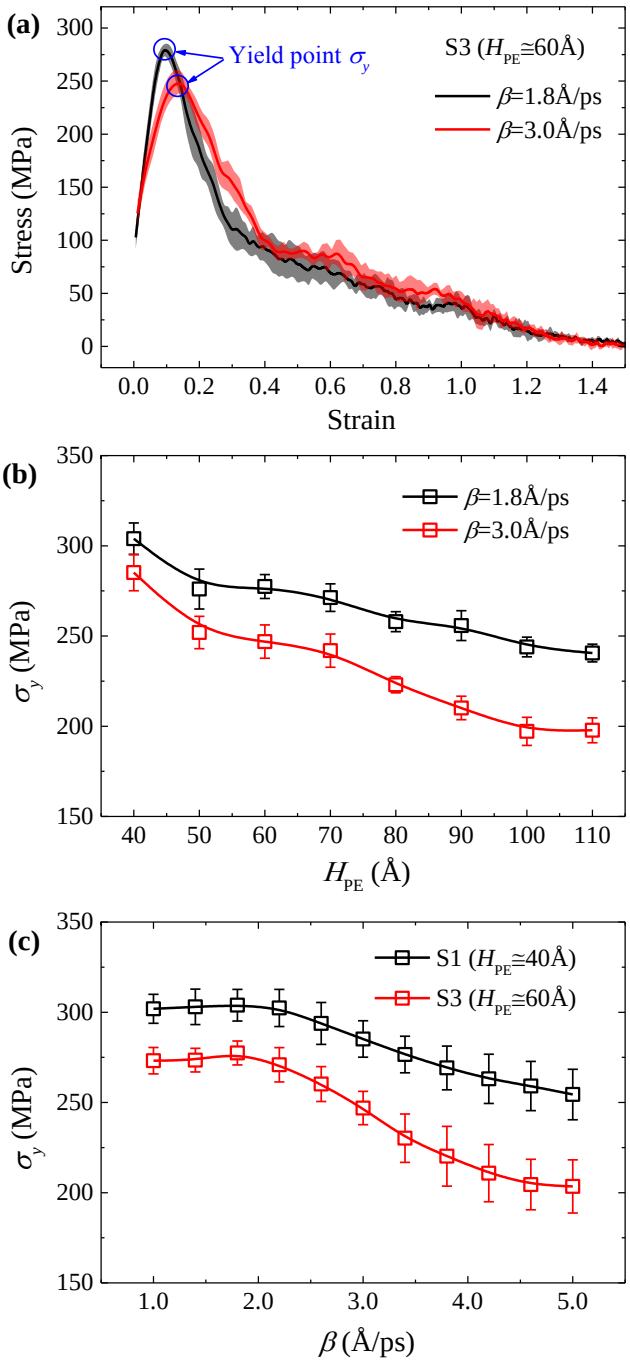

Figure 3. Responses of typical systems under tensile loadings. (a) stress-strain relation of S3 under β=1.8 and 3.0Å/ps, (b) thickness-dependence of yield strength under β=1.8 and 3.0Å/ps, (c) rate-dependence of yield strength of S1 and S3.

simulations on the failure of a glassy polymer confined between rigid walls [30]. In addition, the non-monotonic relation between the yield strength σ_y and the loading rate β was observed as the two examples shown in Fig. 3 (c). A slight raise of the yield strength σ_y can be seen as the loading rate β increases with small value less than 2.0Å/ps approximately. Accompanied with the loading rate β raise, σ_y drops obviously in each system Si (i=1, 2, …, 8). Under small loading rate, the system shows the rate-hardening, which is similar to thecharacteristic of bulk PE system [10]. As the loading rate increasing, rate-softening was found gradually. The piecewise effect of rate-dependence indicates that the governing factor on failure mechanism evolves probably from the bulk PE strength (pure material properties only) at lower β to the interfacial bonding strength (combining with the constraint effect) at higher β.

Figure 4 illustrates the variations of the temperature field T with respect to three typical loading rates β (=1.0, 2.6 and 5.0Å/ps) in a sample of S5 (H_{PE}≈80Å) as an example. The evolutions of the microstructure were also presented. The distributions of the two physical characters were discussed by the projection in the yz plane. The temperature field T was calculated according to the velocity field subtracting velocity biases in the z-direction resulting from the tension. The temperature in the region of damage initiation is higher compared with that in other regions. The location of damage initiation determines the failure mode greatly. Accordingly, the distribution of temperature field is assumed to be effective to

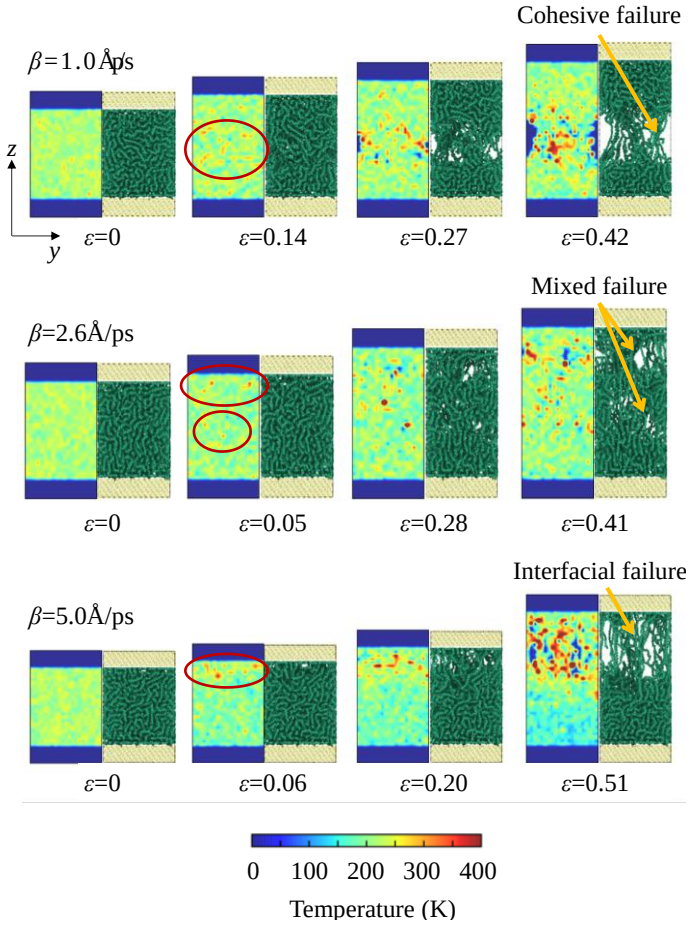

Figure 4. Evolutions of temperature field and microstructure in PE layer of a sample of S5 with respect to loading rate.

predict the failure mode.

Here, cohesive failure indicates that the separation occurs close to the center of the PE layer. The interfacial failure is adopted to describe the debonding-like at the vicinity of PE-copper-interface. The separation at the transition area between the center of PE layer and the interface as mentioned above, the mixed failure was defined. In can be found that the failure mode of the sample examined in Fig. 4 changes from cohesive, mixed and interfacial failure in order gradually as the loading rate increases.

Correspondingly, a parameter λ ranging from 0 to 1 was introduced to predict the position of damage initiation as expressed as $\lambda=m_\lambda/m_0$, where m_λ and m_0 are the PE mass at $\varepsilon=\varepsilon_\lambda$ ($t=t_\lambda$) and at $\varepsilon=0$ ($t=0$) in a certain area near the wall with a height of $H_\lambda=H_{cu}$, respectively. As the schematic picture shown in Fig. 5, it was assumed that the failure mode evolves from interfacial failure ($\lambda\rightarrow 0$) to cohesive one ($\lambda\rightarrow 1$).

The effects of the thickness of PE layer H_{PE} and the loading rate β on the failure mode are summarized in Fig. 5. The result at 5×10^3 time step (5ps) in MD simulation was chosen as an example. The color bar is the average value of λ in each system at 5ps. Figure 5 illustrates that the effect of thickness on the parameter λ strengthens under the loading rate with small values. As the loading rate increasing, the thickness-dependence weakens gradually and diminishes finally. The thicker of the PE layer, the higher value λ can be obtained, which leads to the cohesive failure. Generally, the failure mode evolves from cohesive mode to interfacial one as the loading rate β increases.

Taking the results illustrated in Fig. 3 and Fig. 5 into account simultaneously, it can be observed that the cohesive failure occurs under small loading rate. The failure of the system is mainly governed by the mechanical properties of PE. Accordingly, a rate-hardening was found like the performances of bulk PE examined by previous MD simulations [10] and

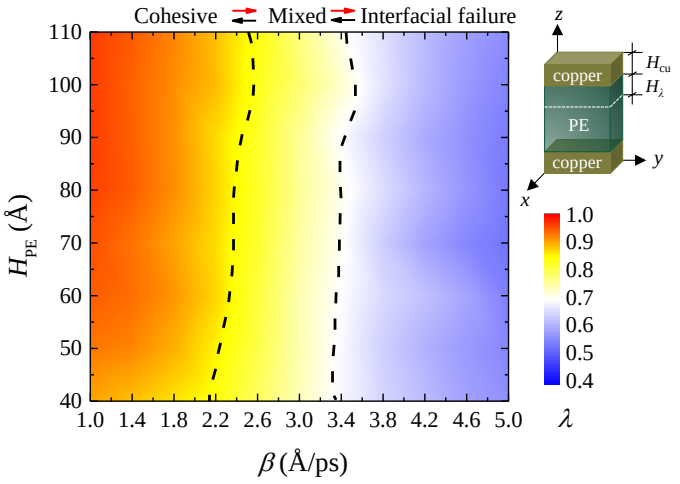

Figure 5. Variation of failure mode of individual system with respect to loading rate at 5ps.

experiments [31]. On the other hand, the failure transfers to the mixed and interfacial mode as the loading rate increases. The structural effect becomes sharply. Accordingly, the coupling effect of material and constraint is assumed to decide the behaviors of the system largely. The bonding strength between PE and copper plays a primary role in the failure gradually, which is inversely proportional to the loading rate with a characteristic of rate-softening.

CONCLUSIONS

In this study, the tensile deformation of a microscale interface between PE and copper was simulated by MD. Moving the copper layer with a given rate, the tensile loading was provided. The effects of thickness of PE layer and the loading rate were discussed. Some conclusions are summarized as follows.

(1) The thickness effect is negative to the load-bearing capacity of the interface. With the characterization of piecewise effect of rate-dependence, the yield strength of the interface is proportional to the lower loading rate and inversely proportional to the higher value with a given thickness of PE layer.

(2) The temperature field is effective to predict the damage initiation and failure mode.

(3) The phase diagram of the failure mode reveals that the failure mode evolves from cohesive failure to interfacial one as the loading rate increases. However, the thickness-dependence on the failure mode is only observed in a narrow range of loading rate with small values.

(4) The material strength of PE decides the failure of interface system largely as the cohesive failure under lower loading rate. Under higher loading rate, the bonding strength between PE and copper governs the failure gradually. The corresponding failure mode changes to the mixed and interfacial one as the loading rate increases progressively.

ACKNOWLEDGMENTS

The authors gratefully acknowledges the support by the National Natural Science Foundation of China grant 11672314. We are also thankful to National Supercomputing Center in Shenzhen (Shenzhen Cloud Computing Center, China) and the Computing Facility, Institute of Mechanics, Chinese Academy of Sciences for supporting the computations.

REFERENCES

1. Pocius, A.V., *Adhesion and Adhesives Technology*. 2012.
2. Adams, R.D., *Adhesive bonding: Science, technology and applications.* Grocery Retailers in Dominican Republic, 2005.
3. Kadam, M. and VVKulkarni. *Finite Element Analysis of simple butt type adhesive joint using RADIOSS*. in *International Conference on Emerging Trends in Engineering, Technology and Architecture*. 2017.

4. Shaikh, S., et al., *Single Lap Adhesive Joint (SLAJ): A Study.* International Journal of Engineering & Technology, 2017(7): p. 64-70.
5. Paz, E., et al., *Influence of Acrylic Adhesive Viscosity and Surface Roughness on the Properties of Adhesive Joint.* Journal of Adhesion, 2017. **92**(11): p. 877-891.
6. Liao, L., T. Sawa, and C. Huang, *Experimental and FEM studies on mechanical properties of single-lap adhesive joint with dissimilar adherends subjected to impact tensile loadings.* International Journal of Adhesion & Adhesives, 2013. **44**(26): p. 91-98.
7. Kramer, E.J. and L.L. Berger, *Fundamental processes of craze growth and fracture*, in *Crazing in Polymers Vol. 2*, H.H. Kausch, Editor. 1990, Springer Berlin Heidelberg: Berlin, Heidelberg. p. 1-68.
8. Fan, H., C.K. Wong, and M.M. Yuen. *A multiscale method to predict delamination in Cu-epoxy systems in electronic packages*. in *Electronic Components and Technology Conference, 2009. ECTC 2009. 59th*. 2009. IEEE.
9. Zhou, X.W., et al., *Molecular-dynamics-based cohesive zone law for brittle interfacial fracture under mixed loading conditions: Effects of elastic constant mismatch.* Acta Materialia, 2009. **57**(16): p. 4671-4686.
10. Hossain, D., et al., *Molecular dynamics simulations of deformation mechanisms of amorphous polyethylene.* Polymer, 2010. **51**(25): p. 6071-6083.
11. Tschopp, M.A., et al., *Quantifying Parameter Sensitivity and Uncertainty for Interatomic Potential Design: Application to Saturated Hydrocarbons.* 2018. **4**(1): p. 011004.
12. Ji, G., et al., *Effects of adhesive thickness on global and local Mode-I interfacial fracture of bonded joints.* International Journal of Solids & Structures, 2010. **47**(18–19): p. 2445-2458.
13. Ji, G., Z. Ouyang, and G. Li, *Effects of bondline thickness on Mode-II interfacial laws of bonded laminated composite plate.* International Journal of Fracture, 2011. **168**(2): p. 197-207.
14. Liao, L., C. Huang, and T. Sawa, *Effect of adhesive thickness, adhesive type and scarf angle on the mechanical properties of scarf adhesive joints.* International Journal of Solids & Structures, 2013. **50**(25–26): p. 4333-4340.
15. Pardoen, T., et al., *Constraint effects in adhesive joint fracture.* Journal of the Mechanics and Physics of Solids, 2005. **53**(9): p. 1951-1983.
16. Yang, S., F. Gao, and J. Qu, *A molecular dynamics study of tensile strength between a highly-crosslinked epoxy molding compound and a copper substrate.* Polymer, 2013. **54**(18): p. 5064-5074.
17. Stukowski, A., *Visualization and analysis of atomistic simulation data with OVITO-the Open Visualization Tool.* Modelling and Simulation in Materials Science and Engineering, 2009. **18**(6): p. 2154-2162.
18. Martínez, L., et al., *PACKMOL: a package for building initial configurations for molecular dynamics simulations.* Journal of Computational Chemistry, 2009. **30**(13): p. 2157-64.
19. Plimpton, S., *Fast parallel algorithms for short-range molecular dynamics.* Journal of Computational Physics, 1995. **117**(1): p. 1-19.
20. Shepherd, J.E., *Multiscale modeling of the deformation of semi-crystalline polymers.* 2006.
21. Huang, L., et al., *Fracture mechanism of amorphous polymers at strain fields.* Physical Chemistry Chemical Physics, 2014. **16**(45): p. 24892-24898.
22. Heinz, H., et al., *Accurate Simulation of Surfaces and Interfaces of Face-Centered Cubic Metals Using 12−6 and 9−6 Lennard-Jones Potentials.* Journal of Physical Chemistry C, 2008. **112**(44): p. 17281-17290.
23. Tran, A.V. and Y. Wang, *Reliable Molecular Dynamics: Uncertainty quantification using interval analysis in molecular dynamics simulation.* Computational Materials Science, 2017. **127**: p. 141-160.
24. Paul, W., D.Y. Yoon, and G.D. Smith, *An optimized united atom model for simulations of polymethylene melts.* The Journal of Chemical Physics, 1995. **103**(4): p. 1702-1709.
25. Capaldi, F.M., M.C. Boyce, and G.C. Rutledge, *Molecular response of a glassy polymer to active deformation.* Polymer, 2004. **45**(4): p. 1391-1399.
26. Kim, J.M., R. Locker, and G.C. Rutledge, *Plastic Deformation of Semicrystalline Polyethylene under Extension, Compression, and Shear Using Molecular Dynamics Simulation.* Macromolecules, 2014. **47**(7): p. 2515-2528.
27. Lavine, M.S., N. Waheed, and G.C. Rutledge, *Molecular dynamics simulation of orientation and crystallization of polyethylene during uniaxial extension.* Polymer, 2003. **44**(5): p. 1771-1779.
28. Lu, T.Y., et al., *Thermal transport in semicrystalline polyethylene by molecular dynamics simulation.* Journal of Applied Physics, 2018. **123**(1).
29. Wang, Y. and L.X. Zhang, *Steered molecular dynamics simulation of elastic behavior of adsorbed single polyethylene chains.* Journal of Polymer Science Part B-Polymer Physics, 2007. **45**(16): p. 2322-2332.
30. Kulmi, U. and S. Basu, *A molecular dynamics study of the failure modes of a glassy polymer confined between rigid walls.* Modelling and Simulation in Materials Science and Engineering, 2006. **14**: p. 1071-1093.
31. Jordan, J.L., et al., *Mechanical Properties of Low Density Polyethylene.* Journal of Dynamic Behavior of Materials, 2016. **2**: p. 1-10.